frontiers | Frontiers in Neurology

TYPE Methods
PUBLISHED 03 August 2023
DOI 10.3389/fneur.2023.1205426

OPEN ACCESS

EDITED BY
Md Nasir Uddin,
University of Rochester, United States

REVIEWED BY
Jianhui Zhong,
University of Rochester, United States
Agnieszka Z. Burzynska,
Colorado State University, United States

*CORRESPONDENCE
Mustapha Bouhrara
✉ bouhraram@mail.nih.gov

†These authors have contributed equally to this work

RECEIVED 13 April 2023
ACCEPTED 14 July 2023
PUBLISHED 03 August 2023

CITATION
Alsameen MH, Gong Z, Qian W, Kiely M, Triebswetter C, Bergeron CM, Cortina LE, Faulkner ME, Laporte JP and Bouhrara M (2023) C-NODDI: a constrained NODDI model for axonal density and orientation determinations in cerebral white matter.
Front. Neurol. 14:1205426.
doi: 10.3389/fneur.2023.1205426

C-NODDI: a constrained NODDI model for axonal density and orientation determinations in cerebral white matter

Maryam H. Alsameen†, Zhaoyuan Gong†, Wenshu Qian, Matthew Kiely, Curtis Triebswetter, Christopher M. Bergeron, Luis E. Cortina, Mary E. Faulkner, John P. Laporte and Mustapha Bouhrara*

Laboratory of Clinical Investigation, National Institute on Aging, National Institutes of Health, Baltimore, MD, United States

Purpose: Neurite orientation dispersion and density imaging (NODDI) provides measures of neurite density and dispersion through computation of the neurite density index (NDI) and the orientation dispersion index (ODI). However, NODDI overestimates the cerebrospinal fluid water fraction in white matter (WM) and provides physiologically unrealistic high NDI values. Furthermore, derived NDI values are echo-time (TE)-dependent. In this work, we propose a modification of NODDI, named constrained NODDI (C-NODDI), for NDI and ODI mapping in WM.

Methods: Using NODDI and C-NODDI, we investigated age-related alterations in WM in a cohort of 58 cognitively unimpaired adults. Further, NDI values derived using NODDI or C-NODDI were correlated with the neurofilament light chain (NfL) concentration levels, a plasma biomarker of axonal degeneration. Finally, we investigated the TE dependence of NODDI or C-NODDI derived NDI and ODI.

Results: ODI derived values using both approaches were virtually identical, exhibiting constant trends with age. Further, our results indicated a quadratic relationship between NDI and age suggesting that axonal maturation continues until middle age followed by a decrease. This quadratic association was notably significant in several WM regions using C-NODDI, while limited to a few regions using NODDI. Further, C-NODDI-NDI values exhibited a stronger correlation with NfL concentration levels as compared to NODDI-NDI, with lower NDI values corresponding to higher levels of NfL. Finally, we confirmed the previous finding that NDI estimation using NODDI was dependent on TE, while NDI derived values using C-NODDI exhibited lower sensitivity to TE in WM.

Conclusion: C-NODDI provides a complementary method to NODDI for determination of NDI in white matter.

KEYWORDS

axonal density, white matter, NODDI, aging, MRI

Introduction

Postmortem histological investigations have shown that cerebral tissue undergoes continuous microstructural and architectural changes throughout the lifespan (1–3). It has been suggested that axonal degeneration is among the main sequelae of aging as well as several age-related disorders, with concomitant motor and cognitive declines (4–12). Therefore, it is indispensable to characterize changes in axonal density that occur with normative aging to identify alterations arising from pathological manifestations. Whilst providing insights into cerebral gray matter (GM) and white matter (WM) maturation and degeneration, histological investigations cannot be performed in real-time on living subjects precluding longitudinal evaluations of brain aging, correlative studies with physical and cognitive performance, or interventions.

Magnetic resonance imaging (MRI), particularly diffusion tensor imaging (DTI), has been extensively used to investigate brain maturation and degeneration, suggesting complex and nonlinear trajectories of the DTI-based indices with age in WM and GM (13–31). Although DTI-indices are sensitive to the fraction of intracellular water, a proxy of axonal density, they are also sensitive to other tissue properties, such as fiber crossing and fanning, while lacking specificity to different diffusion tissue compartments. To overcome this difficulty, the neurite orientation dispersion and density imaging (NODDI) MRI technique has been introduced, providing measures of neurite density and dispersion through computation of the orientation dispersion index (ODI) and the neurite density index (NDI) (32). NODDI has been extensively used in clinical and preclinical studies of aging, neurological disorders, and cognitive function (33–54). However, NODDI-based studies of axonal density and dispersion with normative aging remain limited, and with disparate results. Indeed, Billiet and colleagues and Chang and colleagues observed higher NDI values with age in several cerebral WM regions (43, 44), Merluzzi and colleagues' observed lower NDI values in different cerebral WM structures (46), while Qian and colleagues, Lawrence and colleagues, and Beck and colleagues have recently shown a complex regional association between NDI and age, with several cerebral structures exhibiting inverted U-shaped relationships (6, 7, 55). These observations suggest an increase in axonal density until middle age followed by a loss afterwards (6, 7). It remains unclear whether this discrepancy is due to differences in cohort characteristics or the experimental implementation of NODDI, including variations in echo-time (TE) (56).

NODDI is based on a multicompartmental model of water diffusion incorporating intracellular water, that is, water within neurites, extracellular water, and a compartment consisting of less restricted water from the cerebrospinal fluid (CSF) volume. Although NODDI has gained rapid popularity, criticisms were raised for its overestimation of the isotropically diffusing water fraction (f_{iso}) of the CSF compartment and for providing unrealistically high NDI values in WM (32, 56, 57). Newly, Gong and colleagues have shown that derived NDI values from NODDI are dependent on the echo time (TE) (56). These drawbacks, hampering result interpretation and precluding multisite comparisons, are believed to be due to the underlying assumption in the original NODDI signal model where all compartments are considered to have similar transverse relaxation (T_2) values (56, 57). Indeed, in recent works, Bouyagoub and colleagues have suggested rescaling f_{iso} using predetermined T_2 values of the CSF and intra/extracellular water compartments (57), while Gong and colleagues proposed a multi-echo time NODDI (MTE-NODDI) approach incorporating several NODDI scans performed at different TEs (56). Although these compelling advanced approaches have led to plausible NDI values in WM, they require a lengthy extension of the total scan time making them hardly practical in clinical setting.

In this work, we propose a modification of NODDI that requires no extension of the acquisition time. Our approach is based on the modification of the NODDI signal model such that f_{iso} is provided as an input (i.e., constrained) value in each voxel. This bicomponent model simplifies the tricomponent model used in the original NODDI. We named this approach: constrained NODDI (C-NODDI). Unlike MTE-NODDI, C-NODDI assumes identical T_2 values for both the intra and extra-cellular waters, in line with Bouyagoub and colleagues' original formulation (57). Indeed, this assumption is supported by extensive evidence from previous relaxometry studies, demonstrating that the relaxation times of these two compartments are close (58–61). Using the original NODDI and C-NODDI approaches, we investigated age and sex-related microstructural alterations in WM in a cohort of 58 cognitively unimpaired adults. Further, we compared the correlations between NDI derived values using NODDI or C-NODDI with the neurofilament light chain (NfL) concentration levels, a plasma biomarker of axonal degeneration (62–66), obtained from a subset of 43 participants included in our study cohort. Finally, we investigated the sensitivity of derived NDI and ODI values using NODDI or C-NODDI to TE in two participants from diffusion imaging data acquired at different TEs.

Materials and methods

Participants

Participants underwent a battery of cognitive tests and those with cognitive impairment, metallic implants, neurologic, or significant medical disorders were excluded (67). The final cohort consisted of 58 cognitively unimpaired volunteers (mean ± standard deviation of Mini-Mental State Examination (MMSE) = 29.2 ± 1.0) ranging in age from 21 to 83 years (45.4 ± 18.3 years), including 31 men (42.9 ± 17.5 years) and 27 women (48.3 ± 19.1 years). Age and MMSE did not differ significantly between men and women. The distribution of the number of participants per age decade and sex is shown in Figure 1. Experimental procedures were performed in compliance with our local Institutional Review Board, and participants provided written informed consent.

Data acquisition

All experiments were performed with a 3T whole body Philips MRI system (Achieva, Best, The Netherlands) using the internal

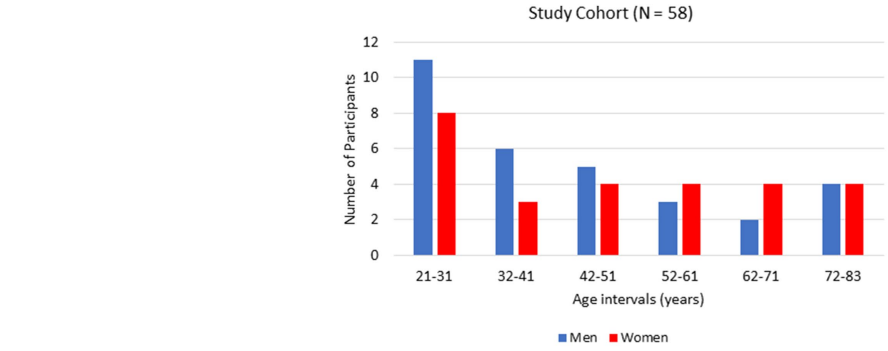

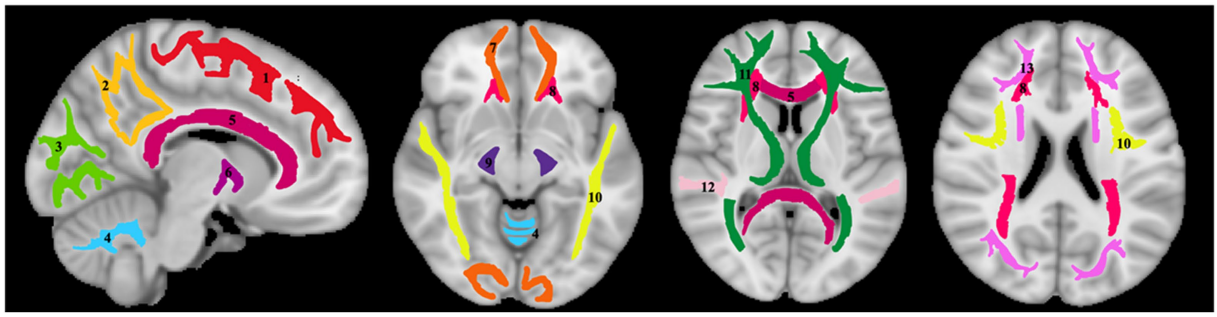

FIGURE 1
Upper panel: number of participants per age decade and sex within the study cohort. Lower panel: visualization of the white matter ROIs used in our analysis. (1) Frontal lobes (FL), (2) parietal lobes (PL), (3) occipital lobes (OL), (4) cerebellum (CRB), (5) corpus callosum (CC), (6) internal capsules (IC), (7) forceps (FR), (8) corona radiata (CR), (9) cerebral peduncles (CP), (10) longitudinal fasciculus (LF), (11) thalamic radiation (TR), (12) temporal lobes (TL), (13) fronto-occipital fasciculus (FOF).

quadrature body coil for transmission and an eight-channel phased-array head coil for reception. Diffusion-weighted images (DWI) were acquired using a single-shot EPI sequence with repetition time (TR) of 10 s, echo time (TE) of 67 ms, three *b*-values of 0, 700, and 2000 s/mm^2, with the two later encoded in 32 diffusion-weighting gradient directions, field-of-view (FoV) of 240 mm × 208 mm × 150 mm, acquisition matrix of 120 × 120 × 50, and acquisition voxel size of 2 mm × 2 mm × 3 mm. Images were acquired with SENSE factor of 2 and reconstructed to a voxel size of 2 mm × 2 mm × 2 mm. The total acquisition time was ~16 min.

Finally, to evaluate the effect of TE on NDI and ODI derived using NODDI or C-NODDI, DW images were acquired from the brains of two participants at four different TEs of 78, 90, 100 or 120 ms. Here again, three *b*-values of 0, 700, and 2000 s/mm^2 were acquired, with the two later encoded in 32 diffusion-weighting gradient directions sampling the same *q*-space, FoV of 240 mm × 208 mm × 150 mm, acquisition matrix of 120 × 120 × 50, and acquisition voxel size of 2 mm × 2 mm × 3 mm.

The C-NODDI signal model

Signal model

NODDI is a multicompartmental signal model of water diffusion incorporating intracellular water, extracellular water and CSF water volumes (32). Assuming that each of these three compartments exhibits unique transverse and longitudinal relaxation times and diffusion coefficient, the signal model can be expressed as:

$$S = S_0 \left[\begin{array}{l} f_{in} e^{-\frac{TE}{T_{2,in}}} \left(1 - e^{-\frac{TR}{T_{1,in}}} \right) S_{D,in} + f_{ex} e^{-\frac{TE}{T_{2,ex}}} \left(1 - e^{-\frac{TR}{T_{1,ex}}} \right) S_{D,ex} \\ + f_{iso} e^{-\frac{TE}{T_{2,iso}}} \left(1 - e^{-\frac{TR}{T_{1,iso}}} \right) S_{D,iso} \end{array} \right] \quad (1)$$

where S is the measured signal at a given combination of TE, repetition time (TR) and *b*-value; S_0 is the signal at TE = 0 ms with TR = +∞ and *b*-value = 0 s/mm^2; f_{in}, f_{ex} and f_{iso} are, respectively, the fractions of the intracellular, extracellular and CSF water pools; $T_{2,in}$, $T_{2,ex}$ and $T_{2,iso}$ are, respectively, the transverse relaxation times of the intracellular, extracellular and CSF water pools; $T_{1,in}$, $T_{1,ex}$ and $T_{1,iso}$ are, respectively, the longitudinal relaxation times of the intracellular, extracellular and CSF water pools; and $S_{D,in}$, $S_{D,ex}$ and $S_{D,iso}$ are, respectively, the signal attenuation due to water diffusion of the intracellular, extracellular and CSF water pools. When long TR is applied (e.g., TR >> T_1), the T_1 effect is mitigated so that Eq. 1 can be reduced to:

$$\frac{S}{S_0} = f_{in} e^{-\frac{TE}{T_{2,in}}} S_{D,in} + f_{ex} e^{-\frac{TE}{T_{2,ex}}} S_{D,ex} + f_{iso} e^{-\frac{TE}{T_{2,iso}}} S_{D,iso} \quad (2)$$

Furthermore, it has previously been shown that $T_{2,in} \approx T_{2,ex} = T_{2,in/ex}$ (58–61), in which case Eq. 2 can be reduced to:

$$A = f_{in}S_{D,in} + f_{ex}S_{D,ex} + F_{iso}S_{D,iso} \quad (3)$$

where $A = S / S_{b=0}$ is the measured normalized diffusion-weighted signal, with $S_{b=0} = S_0 \exp(-TE / T_{2,in/ex})$ representing the T_2-weigthed image obtained at b-value of 0 s/mm^2, and $F_{iso} = f_{iso} \exp(-TE / T_{2,iso} + TE / T_{2,in/ex})$. In voxels with no CSF contamination such as the deep WM regions, $F_{iso} = 0$ so that Eq. 3 can be reduced to $A = f_{in}S_{D,in} + (1 - f_{in})S_{D,ex}$, in which case, derived NDI (i.e., f_{in}) values are expected to be relatively independent of T_2 and, therefore, are also relatively independent of the choice of TE. However, in regions with CSF contamination, i.e., $F_{iso} > 0$, which must be estimated.

It must be emphasized that C-NODDI relies on the strong assumption that the transverse relaxation times of the intracellular and extra-cellular waters exhibit similar values. However, separation in relaxation times between intracellular and extracellular water compartments remains an open area of investigation. While relaxometry-based studies consistently indicate minimal differences in these transverse relaxation times despite employing different acquisition strategies and fitting approaches (58–60, 68), some diffusion-relaxometry-based studies suggest the potential for discrepant values (56, 69).

NDI and ODI mapping

In the original NODDI approach, F_{iso} is derived along with NDI and ODI (32). We modified the NODDI MATLAB toolbox[1] so that F_{iso} is instead provided as a known input parameter. This strategy allows a reduction of the number of unknown parameters to be estimated (Eq. 3), thus restricting the parameter space and improving the fitting stability of the C-NODDI signal model (70–73). Here, the F_{iso} map is computed from the T_2-weigthed image obtained at b-value of 0 s/mm^2 using the hidden Markov random field model and the expectation–maximization algorithm (74), known as FAST in the FSL software (75). FAST segments a structural image of the brain into different tissue classes, including WM, GM and CSF/F_{iso}, providing, in each voxel, estimates of the fractions of these tissue compartments. Extensive work has previously been conducted to evaluate the accuracy of FAST for tissue segmentation (76–78). The derived F_{iso} map is then used as an input to calculate NDI and ODI using our modified NODDI approach, C-NODDI. All MATLAB codes are available upon request from the corresponding author.

For each participant, corresponding NDI and ODI maps were generated using NODDI and C-NODDI. Specifically, all DW images were registered to the b_0 image and corrected for motion and eddy current distortion artifacts using the Artefact Correction in Diffusion MRI (ACID) toolbox[2] (79). The co-registered DW images were then used to calculate NDI and ODI using NODDI or C-NODDI.

1 https://www.nitrc.org/projects/noddi_toolbox

2 http://diffusiontools.com/

Regions-of-interest determination

For each participant, using FSL, the DW image obtained with b of 0 s/mm^2 was nonlinearly registered to the Montreal Neurological Institute (MNI) standard space and the derived transformation matrix was then applied to the corresponding NDI and ODI maps. Fourteen WM regions of interest (ROIs) were defined from MNI encompassing the whole brain (WB), frontal lobes (FL), parietal lobes (PL), temporal lobes (TL), occipital lobes (OL), cerebellum (CRB), corpus callosum (CC), internal capsules (IC), cerebral peduncle (CP), corona radiata (CR), thalamic radiation (TR), fronto-occipital fasciculus (FOF), longitudinal fasciculus (LF), and forceps (FR), as shown in Figure 1. All ROIs were eroded to reduce partial volume effects and imperfect image registration using the FSL tool *fslmaths*. Finally, the mean NDI and ODI values within each ROI were calculated.

Analyses

Differences in F_{iso}

In this analysis, we compared derived F_{iso} maps using NODDI or FAST. Derived F_{iso} maps were shown for a representative example. The goal here is to demonstrate the overestimation of F_{iso} from NODDI, and to evaluate the performance of FAST in F_{iso} determination.

Differences in NDI and ODI

In this analysis, we compared NDI and ODI maps derived using NODDI or C-NODDI. Average NDI and ODI maps by age intervals over the adult lifespan for a representative axial slice were calculated. Furthermore, to investigate the effects of age and sex on NDI and ODI, multiple linear regression analysis was applied using the mean NDI or ODI derived from NODDI or C-NODDI within each ROI as the dependent variable and sex, age, and age^2 as the independent variables, after mean age centering. In all cases, the interactions between sex and age or age^2 were found to be nonsignificant and were therefore omitted from the parsimonious model. Further, for each ROI, Pearson correlation analysis was conducted to examine the discrepancy between ODI, or NDI, values derived using NODDI or C-NODDI. For all analyses, the threshold for statistical significance was $p < 0.05$ after correction for multiple ROI comparisons using the FDR method (80, 81). FDR correction was conducted across ROIs for each MRI metric.

Correlations of NDI and NfL

In this analysis, we assessed the correlations between NDI derived using NODDI or C-NODDI and NfL which represents a plasma biomarker of axonal degeneration (62–66). NfL was measured from 43 participants of our study cohort (age: 50 [SD 18]). Blood for plasma biomarker measurement was collected at the time of MRI. Plasma was separated, aliquoted and stored at −80°C using standardized protocols. EDTA plasma was used to measure NfL using the Quanterix Single Molecule Array (Simoa) Neurology 4-Plex E assay on the HD-X Instrument (Quanterix Corporation). NfL was used as the dependent variable and NDI as the independent variables while accounting for age and sex as relevant covariates. The regression model is given by:

10.3389/fneur.2023.1205426

$$\mathrm{NFL}_i \sim \beta_0 + \beta_{NDI} \times \mathrm{NDI}_i + \beta_{age} \times \mathrm{age}_i + \beta_{sex} \times \mathrm{sex}_i,$$

where β is the regression coefficients and i is the index of i^{th} subject. NfL values were log-transformed to remove the skewness of their distributions. Further, to facilitate results interpretation, the NfL and NDI indices were Z-scored by calculating the mean (μ) and standard deviation (σ) separately for NfL and NDI variables in the full study sample using the formula $z = (x - \mu)/\sigma$.

Effect of TE

To investigate the effect of TE on derived NDI and ODI values using C-NODDI or NODDI, parameter maps as well as mean values calculated over a large WM region encompassing the cerebral lobes, at each TE, were displayed for two participants.

Results

Figure 2 shows representative F_{iso} maps derived using NODDI or FAST/FSL. It is readily seen that th F_{iso} map derived using NODDI exhibits abnormally high F_{iso} values, especially within several WM regions, with values reaching over 0.25 (i.e., 25%) in several voxels. In contrast, derived F_{iso} values using the hidden Markov random field model and the expectation–maximization algorithm, the FAST algorithm as implemented in FSL, are within the physiologically expected ranges with values near zero in the deep WM regions.

Figure 3 shows representative average NDI and ODI maps for different age intervals corresponding to young, middle, late middle and late adulthood. Visual inspection indicates increases in NDI values from early adulthood through middle age (i.e., 40–59 years), followed by lower NDI values in several brain regions, consistent with progressive increases in axonal density followed by reductions at older ages. Furthermore, we note that different regions exhibit different patterns in the association of NDI with age. In contrast, the ODI maps exhibit low regional variations with age. Remarkably, NDI maps derived from NODDI exhibit values that exceed 0.7 (i.e., 70%) in several cerebral WM structures, while the NDI values derived using C-NODDI are considerably lower. Moreover, ODI maps derived using NODDI and C-NODDI were virtually identical. Indeed, our quantitative comparison, presented in Figure 4, indicates weak to moderate regional Pearson correlation between the NDI values derived using NODDI and those derived using C-NODDI for all ROIs investigated, in agreement with visual inspection (Figure 3). In contrast, strong regional correlations were observed between the ODI values derived from the two NODDI approaches.

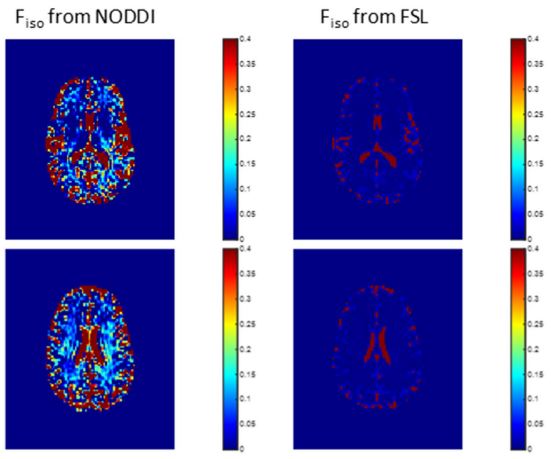

FIGURE 2
Representative maps of the fraction of the isotropic diffusion component F_{iso}, that is, the cerebrospinal fluid fraction, derived using NODDI (left) or using the FAST algorithm as implemented in the FSL software (right). Results are shown for three representative slices. It is readily seen that the NODDI approach overestimates F_{iso}, especially in the white matter regions.

Figures 5, 6 show, respectively, quantitative results for the NDI and ODI values calculated using NODDI or C-NODDI from all participants as a function of age for the indicated 14 WM regions. These results show, in agreement with Figures 3, 4, increasing NDI until middle age followed by decreases afterward in most examined ROIs, with the best-fit curves displaying regional variation. Remarkably, the quadratic effect of age on NDI derived using C-NODDI was readily observable in almost all ROIs, as compared to the NDI results derived using NODDI which was limited to a few. Furthermore, in agreement with Figures 3, 4, ODI values derived using either NODDI approach exhibited similar regional trends that were, overall, constant with age with limited ROIs exhibiting either increasing or decreasing trends. In agreement with visual inspection, statistical analysis indicates that the quadratic effect of age, age^2, on NDI derived using C-NODDI was significant ($p < 0.05$) in several ROIs, while this effect on NDI derived using NODDI was limited to a few ROIs (Table 1). For both NODDI approaches, the quadratic effect of age on ODI was not significant. In contrast, the effect of age on NDI-C-NODDI was significant in almost all ROIs, while the age effect on NDI-NODDI was observed in only three ROIs. For both NODDI approaches, the effect of age on ODI was only significant in very limited cerebral regions. In addition, the effect of sex on NDI or ODI was, overall, not significant. Finally, in all ROIs, the NDI-C-NODDI results exhibited peak values at younger ages, as compared to the NDI results derived using NODDI.

Our multiple regression between NDI and NfL indicates stronger correlations between NDI-C-NODDI vs. NfL as compared to NDI-NODDI vs. NfL, with lower NDI values corresponding to higher NfL concentration levels in all ROIs investigated (Figure 7). We also note that the negative trend between NDI and NfL was observed in all brain regions except in the cerebral peduncles (data not shown).

Finally, Figures 8, 9 show, respectively, examples of derived NDI and ODI maps and mean parameter values calculated over the whole WM region using NODDI or C-NODDI at several TEs using DWI data acquired from the brains of two participants. Visual inspection and quantitative analysis indicate that derived NDI estimates using NODDI are TE-dependent exhibiting increased values with TE increases. In contrast, the NDI maps and mean values calculated using C-NODDI exhibit lower dependence on TE. However, although the majority of the white matter regions exhibited relatively lower dependence on TE, some regions showed substantially increased values with TE. Further, it is readily seen that the ODI maps calculated using NODDI or C-NODDI are similar and with mean values virtually constant as a function of TE. Moreover, we note that derived NDI and ODI maps exhibit some regional differences across TEs; this is due to differences in signal-to-noise ratio due to differences in TEs leading

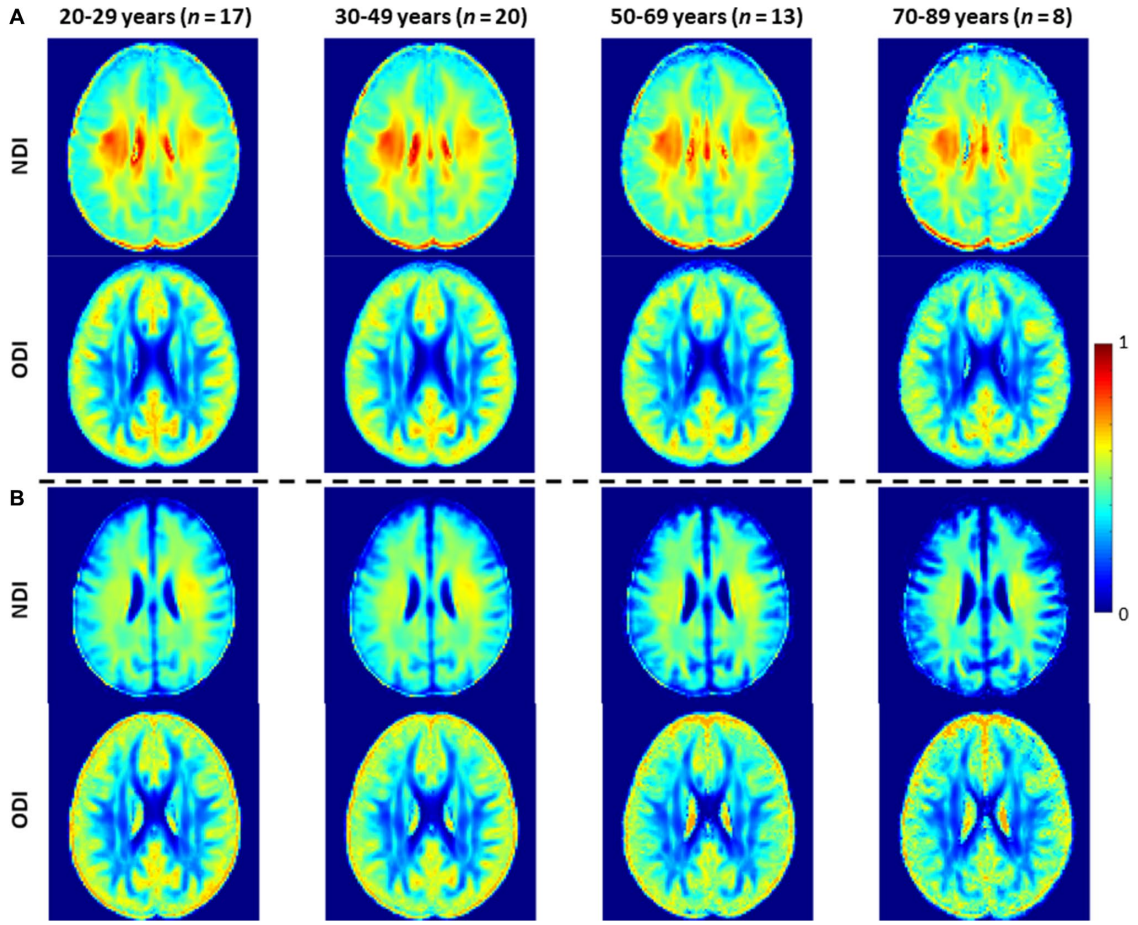

FIGURE 3
NDI and ODI maps represented as averaged participant maps calculated over four age intervals. Results are shown for a representative slice. NDI and ODI maps derived **(A)** using the original NODDI approach, and **(B)** using the C-NODDI approach. While the ODI values derived using both approaches are virtually identical, C-NODDI provides substantially lower NDI values than those derived using NODDI.

to signal drops at higher TEs, as well as to some persisting image misregistration.

Discussion and conclusion

In this work, we introduced a modification of the NODDI signal model, C-NODDI, to overcome documented problems with the original NODDI approach. Specifically, this modification addresses the overestimations of the CSF and NDI fractions in WM. Our results show that C-NODDI provides lower NDI estimates as compared to NODDI and confirm that NODDI provides high NDI values in several WM structures with values over 70% at several cerebral structures in agreement with previous reports (56, 57). NDI values derived from C-NODDI were regionally 20–40% lower than those derived using NODDI; this agrees with Bouyagoub and colleagues' results (57). However, unlike their approach which requires a substantial extension of the total acquisition time, our approach does not require additional acquisition time. Indeed, C-NODDI is based on prior estimation of the signal fraction of the CSF. In this proof-of-concept work, we showed that this fraction can be estimated using the T_2-weigthed image acquired at b-value of 0 s/mm^2 and the hidden Markov random field model and the expectation–maximization algorithm; this allows reduction of the fitting parameter space of the NODDI model (74). Indeed, the NODDI signal model incorporates several parameters to be estimated. Parameter estimation in high dimensional problems, that is, those for which the number of parameters to be estimated is large, is complicated by the presence of local minima and saddle points (73). This problem becomes more acute with the flatness of the least-squares residual surfaces seen with increasing model complexity exhibiting higher sloppiness, that is, different parameter combinations leading to virtually equivalent signal behavior (70–72). However, both NODDI and C-NODDI signal models are just approximations of the underlying biology so that further histological validations are required to assess their reliability and accuracy. We note that the CSF fraction can be estimated using different approaches, including the free-water estimation (FWE) diffusion approaches from the same NODDI dataset, or using FAST from various other structural contrast-weighted images that are routinely acquired in clinical studies (82, 83), or from single shell diffusion (82, 84, 85). A thorough comparison of all these techniques is still needed, especially in the context of their applications to neurodegeneration. Nevertheless, the existing FWE diffusion approaches provide only an estimate of the apparent free

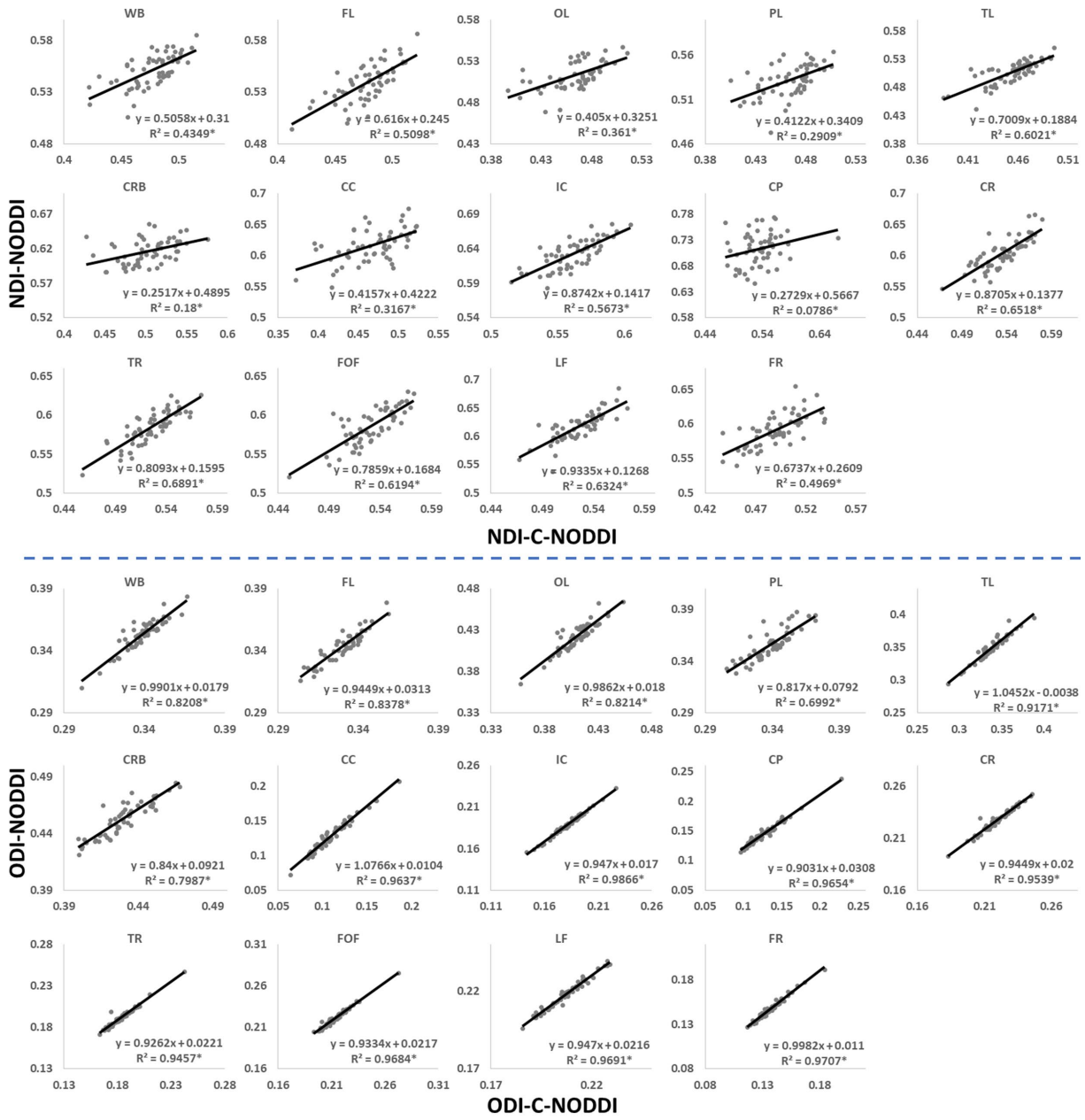

FIGURE 4
Pearson correlations between NDI, or ODI, derived values using C-NODDI and NODDI in the 14 WM ROIs studied. The coefficient of determination is provided with * indicating significant correlation. While derived ODI values using NODDI or C-NODDI were virtually identical exhibiting very high correlation coefficients, the NDI values derived using these two approaches were substantially different with NODDI exhibiting higher NDI values in several WM regions. WB, whole brain; FL, frontal lobes; PL, parietal lobes; TL, temporal lobes; OL, occipital lobes; CRB, cerebellum; CC, corpus callosum; IC, internal capsules; CP, cerebral peduncle; CR, corona radiata; TR, thalamic radiation; FOF, fronto-occipital fasciculus; LF, longitudinal fasciculus; FR, forceps.

water fraction due to the impact of the differential T_2 weighting of the intra/extra and CSF/free water compartments. While MTE-NODDI provides CSF fraction maps that are TE-independent and with values that are relatively lower than those derived using NODDI (Figure 10), their determination is still based on the F_{iso} maps derived using NODDI at each TEs. Therefore, further investigations are needed to assess its reliability. Finally, we note that C-NODDI is in principle similar to a recently introduced technique, DLpN, where the CSF is used as a prior (84). A direct comparison between DLpN and C-NODDI as well as the association of derived NDI values with NfL is of interest and represent a potential direction of the current work.

We investigated the association between NDI or ODI, derived using NODDI or C-NODDI, and age in several cerebral WM structures in a healthy adult population spanning a wide age range. Our results revealed widespread WM microstructural differences as a function of age, as well as regional variations between the NDI or ODI measures and age. Specifically, NDI exhibited quadratic, inverted U-shaped, regional trends with age; this agrees with Beck and colleagues' and our

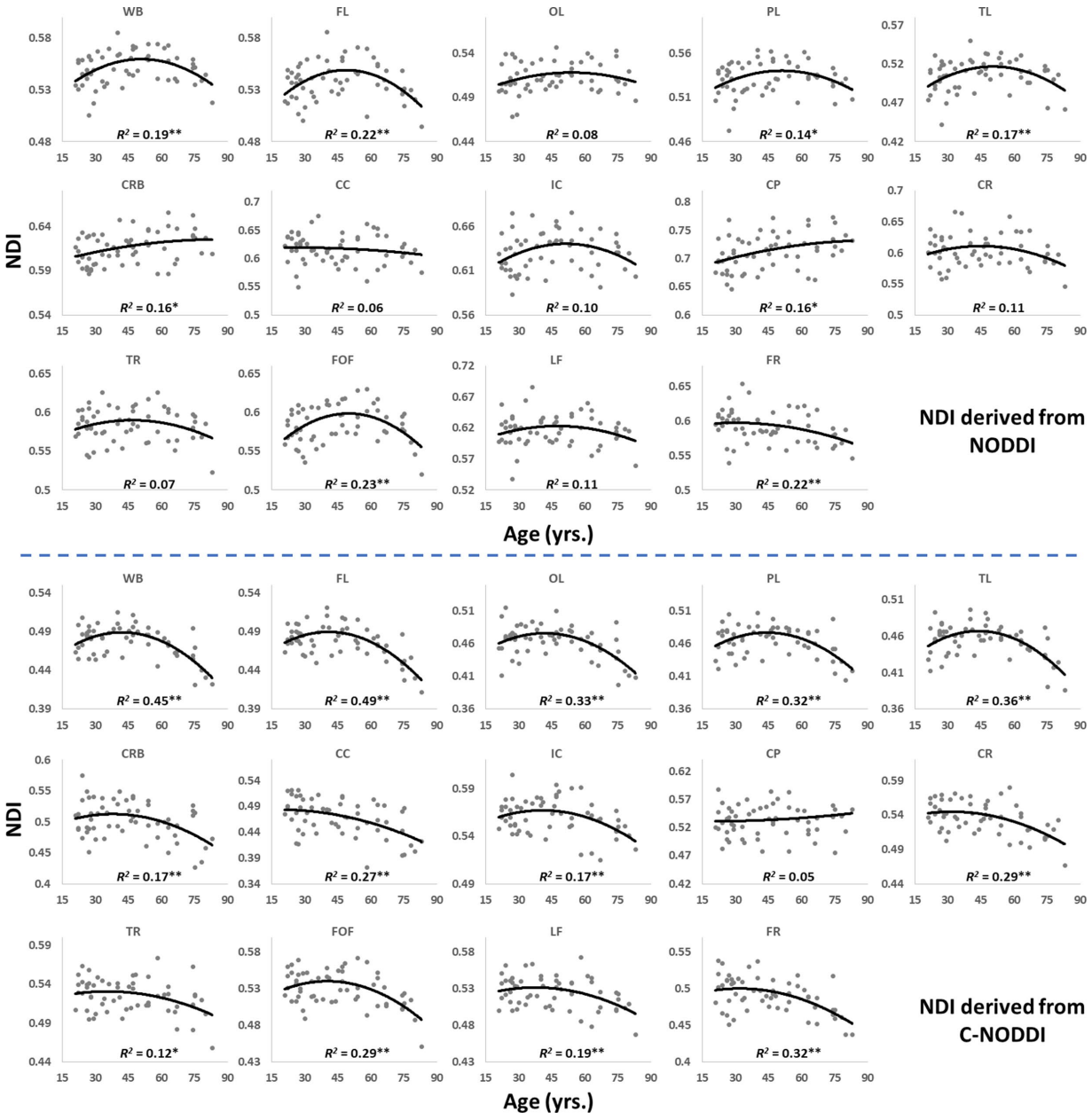

FIGURE 5
Regional NDI values derived using NODDI (top plots) or C-NODDI (bottom plots) as a function of age. Although most regions investigated exhibit inverted U-shaped trends of NDI with age, these quadratic trends were more noticeable and significant for the NDI-C-NODDI results (see Table 1). WB, whole brain; FL, frontal lobes; PL, parietal lobes; TL: temporal lobes; OL, occipital lobes; CRB, cerebellum; CC, corpus callosum; IC, internal capsules; CP, cerebral peduncle; CR, corona radiata; TR, thalamic radiation; FOF, fronto-occipital fasciculus; LF, longitudinal fasciculus; FR, forceps. * indicates $p < 0.05$ while ** indicates $p < 0.01$.

recent results (6, 7) and to some extent with Cox and colleagues' and Laurence and colleagues' observation in a large sample sizes derived from the UK Biobank (55, 86). We attribute this finding to a continuous maturation of axons with an increase in axonal density until middle age, followed by a phase of neurodegeneration and consequence axonal loss at older ages. Interestingly, the quadratic effect of age, age^2, on NDI was significant ($p < 0.05$) in several regions investigated using C-NODDI, while this inverted U-shaped association was limited to only a few cerebral regions using the original NODDI approach. Although this observation indicates the potential higher sensitivity of C-NODDI to capturing differences in neurite density with age, further comparison between NODDI and C-NODDI in larger cohorts is still required to confirm or infirm this finding. We note that other investigations have shown either higher or lower NDI values with age in WM (43, 44, 46). This discrepancy is likely due to differences in the characteristics of the study cohorts as well the instability of NODDI. Indeed, Billiet's and Chang's studies, although incorporating wide age ranges, possess only a limited number of subjects over 60 years old, while Merluzzi's cohort included only subjects over 45 years old. These limitations may have precluded the detection of the quadratic

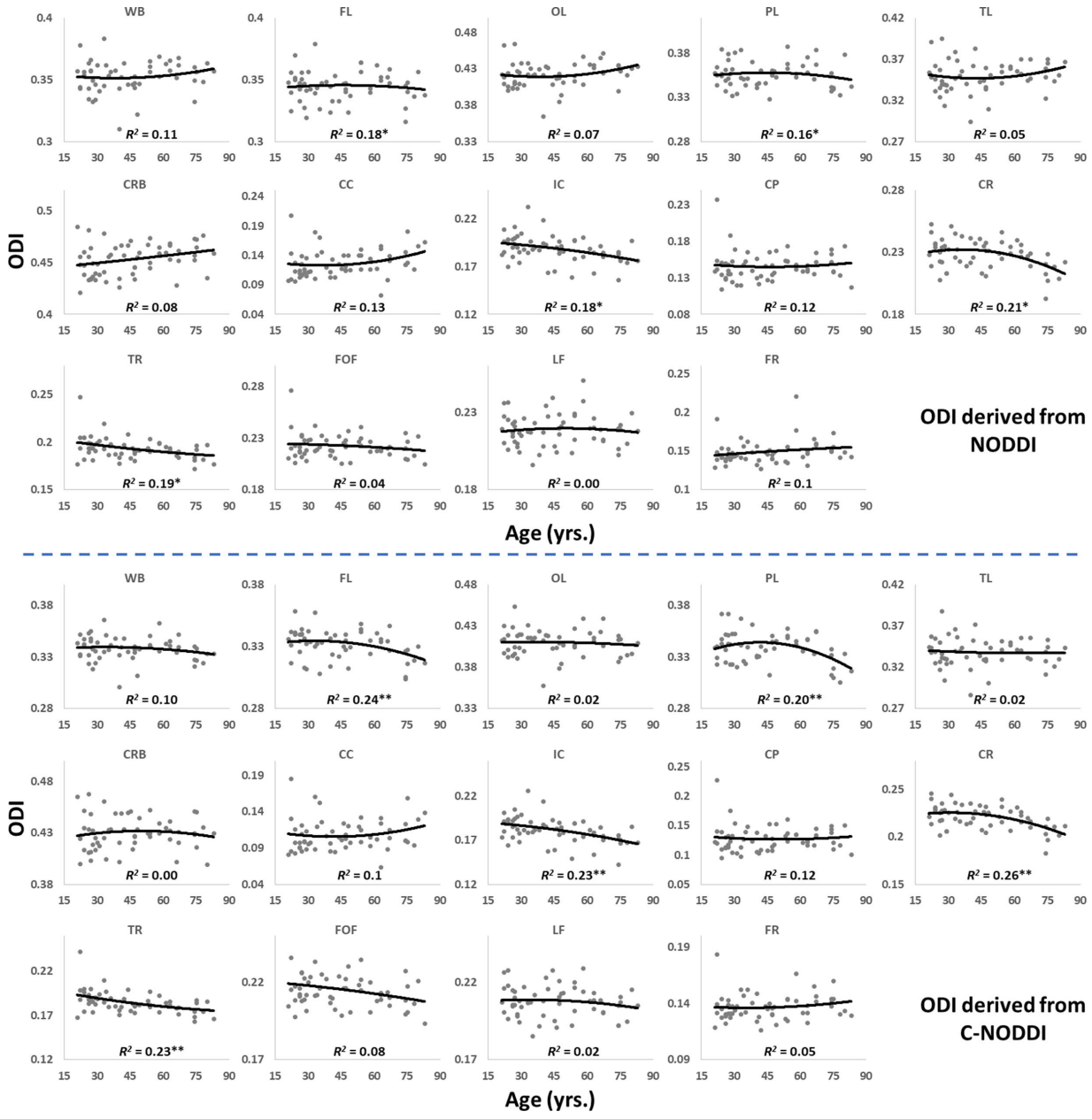

FIGURE 6
Regional ODI values derived using NODDI (top plots) or C-NODDI (bottom plots) as a function of age. Results were very similar for both approaches. WB, whole brain; FL, frontal lobes; PL, parietal lobes; TL, temporal lobes; OL, occipital lobes; CRB, cerebellum; CC, corpus callosum; IC, internal capsules; CP, cerebral peduncle; CR, corona radiata; TR, thalamic radiation; FOF, fronto-occipital fasciculus; LF, longitudinal fasciculus; FR, forceps.

association between NDI and age, that Beck, Lawrence and we have observed (6, 7, 55). This issue may have been exacerbated by differences in the experimental implementation of NODDI given its high sensitivity to TE (56). Further, ODI exhibited non-consistent regional trends with age, with most WM regions exhibiting constant trends while other, but limited, regions exhibited either increasing or decreasing trends. The literature regarding differences in ODI with age remains sparse, necessitating further detailed investigations (6, 43, 44, 46). Finally, our results revealed that elevated concentration levels of NfL were associated with lower NDI values suggesting a role of axonal degeneration in neuroinflammation. This association was stronger between NDI derived using C-NODDI and NfL, suggesting that NDI-C-NODDI could represent a reliable imaging biomarker of axonal integrity. Further studies in larger cohorts and using NfL concentrations derived from CSF are still required.

In all ROIs, NDI calculated using C-NODDI exhibited peak values at much younger ages compared to NDI calculated using NODDI, with differences ranging from ~6 to ~10 years. This indicates that axonal maturation continues until the early fifth decade of age. This finding agrees with results derived using sensitive MRI measures of axonal density, including relaxation times and DTI indices, all indicating that WM tissue maturation continues until the late fourth decade to the early fifth decade of age (15, 16, 18, 87). Interestingly, recent studies have shown that myelination continues until the early

10.3389/fneur.2023.1205426

TABLE 1 Significance of each coefficient incorporated into the linear regression analysis of NDI or ODI derived using NODDI or C-NODDI, and the year of apparent maximum NDI in each ROI.

	NODDI							C-NODDI						
	NDI				ODI			NDI				ODI		
	Age	Sex	Age^2	Year of max NDI	Age	Sex	Age^2	Age	Sex	Age^2	Year of max NDI	Age	Sex	Age^2
WB	–	–	**	50.8	–	–	–	**	–	**	42.3	–	–	–
FL	–	–	**	48.9	–	*	–	**	–	**	41.1	*	–	–
OL	–	–	–	NA	–	–	–	**	–	**	41.8	–	–	–
PL	–	–	*	50.5	–	*	–	**	–	**	44.6	*	–	–
TL	–	–	*	50.3	–	–	–	**	–	**	44.0	–	–	–
CRB	*	–	–	NA	–	–	–	*	–	–	NA	–	–	–
CC	–	–	–	NA	–	–	–	**	–	–	NA	–	–	–
IC	–	–	–	NA	*	–	–	*	–	–	NA	**	–	–
CP	*	–	–	NA	–	–	–	-	–	–	NA	–	–	–
CR	–	–	–	NA	*	–	–	**	–	–	NA	**	–	–
TR	–	–	–	NA	*	–	–	*	–	–	NA	**	–	–
FOF	–	–	**	49.9	–	–	–	**	–	*	40.6	–	–	–
LF	–	–	–	NA	–	–	–	**	–	–	NA	–	–	–
FR	*	–	–	NA	–	–	–	**	–	–	NA	–	–	–

NA indicates "not applicable" for a nonsignificant age^2 term. * Indicates $p < 0.05$, ** indicates $p < 0.01$, and – indicates non-significant effects. All p-values presented are obtained after FDR correction. WB, whole brain; FL, frontal lobes; PL, parietal lobes; TL, temporal lobes; OL, occipital lobes; CRB, cerebellum; CC, corpus callosum; IC, internal capsules; CP, cerebral peduncle; CR, corona radiata; TR, thalamic radiation; FOF, fronto-occipital fasciculus; LF, longitudinal fasciculus; FR, forceps.

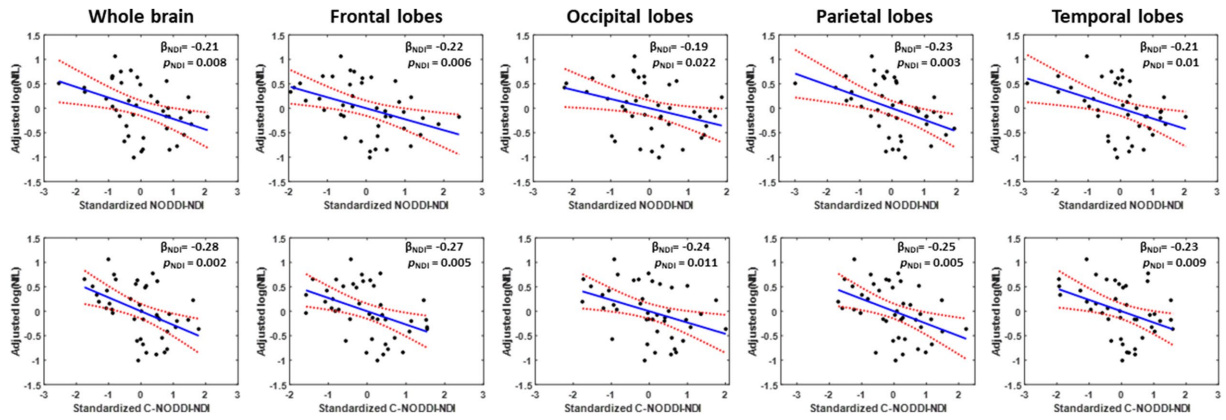

FIGURE 7
Representative correlation plots between neurodegeneration biomarker, NfL, and NDI values derived using NODDI (left plot) or C-NODDI (right plot) from the whole brain, frontal lobes, occipital lobes, parietal lobes, or temporal lobes. Line of fit (in blue), confidence interval lines (red), and the regression coefficient (β_{NDI}) and significance (p_{NDI}) of the NDI variable were displayed.

fifth decade of age as well (17, 88, 89). It has been shown that axonal activity is an important contributing factor in myelin modulation (90, 91). Moreover, aside from acting as an electric insulator, oligodendrocytes, the cells that produce myelin, provide substantial metabolic support to axons (92). Given this physiological coupling between axons and myelination, it is plausible that axonal maturation and myelin maturation follow similar patterns and peak at similar ages. However, further investigations on larger cohorts, in addition to longitudinal studies, are required to derive definite conclusions regarding whether the maturation and myelination pattern of axons are mechanistically associated or represent two independent neurological processes. These studies are crucial for the development of specific interventions supporting myelin maintenance, axonal regeneration, or both simultaneously.

Using data acquired from three participants at different TEs, we confirmed Gong and colleagues' observation that the NDI estimates are dependent on TE, with NDI values increasing with TE (56). However, derived NDI values using C-NODDI exhibited a relatively lower

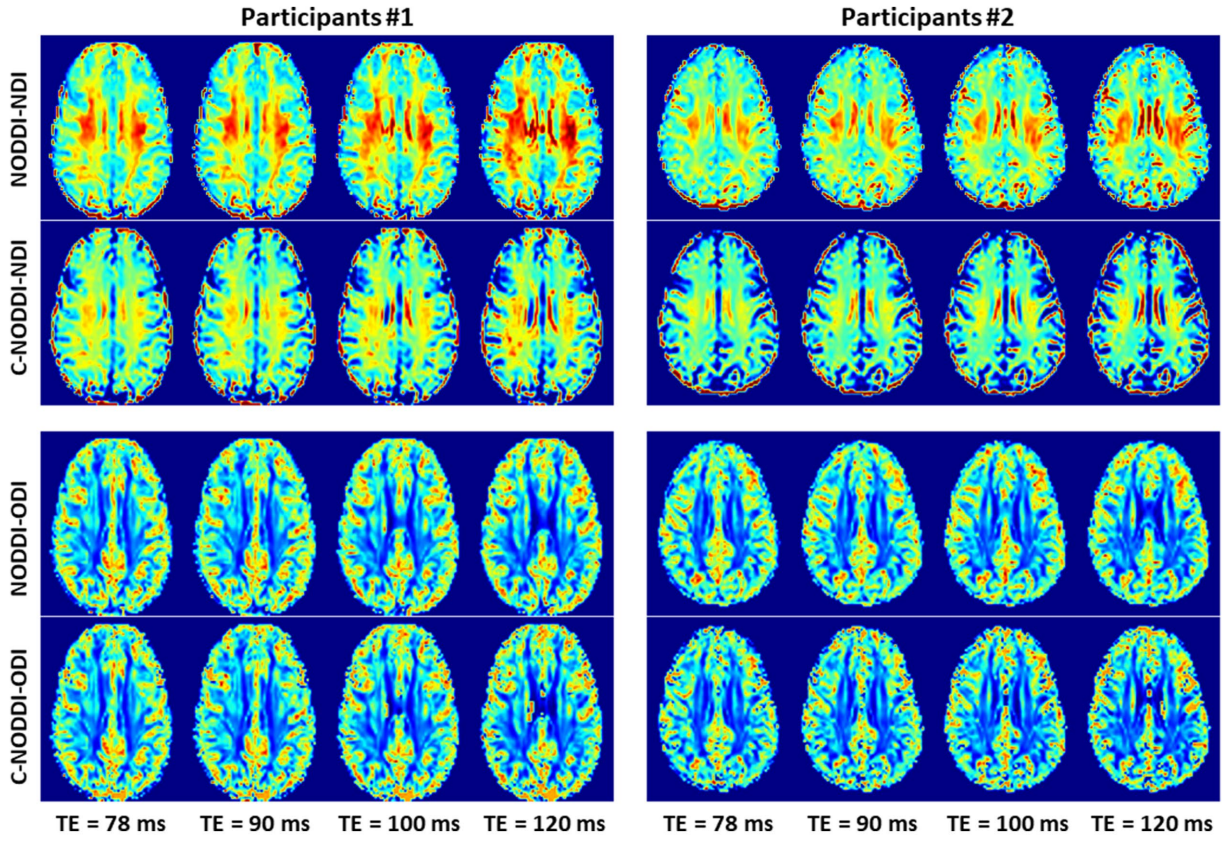

FIGURE 8
NDI and ODI maps derived using NODDI or C-NODDI from DWI data acquired at different TEs from the brains of two different participants. Results are shown for a representative slice for each of the participants.

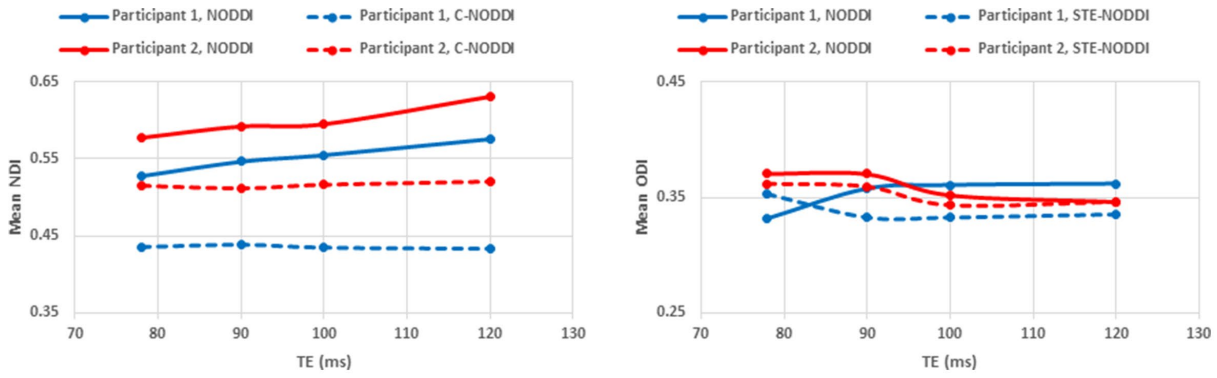

FIGURE 9
Mean NDI values and ODI values calculated from a large WM region encompassing the cerebral lobes, derived using NODDI or C-NODDI as a function of TE. It is readily seen from this quantitative analysis that the NDI values derived using NODDI increase with TE, while derived ODI values using either approach are relatively similar between both approaches with, overall, constant or decreasing trends as a function of TE, in agreement with the visual inspection (Figure 8).

dependence on TE in several WM structures. We believe that the artificial overestimation of the CSF fraction using NODDI is a leading factor of the strong underlying TE-dependency observed previously, particularly in WM. It is important to note that certain WM regions still exhibited TE-dependency in C-NOODI, with relatively higher values observed at increasing TE. Thus, further examination of the effect of T_2s on derived diffusion parameters is required as well as a comprehensive comparison of these approaches under different experimental designs, including in terms of different ranges and numbers of TEs and *b*-values. Furthermore, in perfect agreement with Bouyagoub's and Gong's results (56, 57), we found that ODI values derived using NODDI or C-NODDI were virtually identical, as expected. Since the calculation of ODI does not

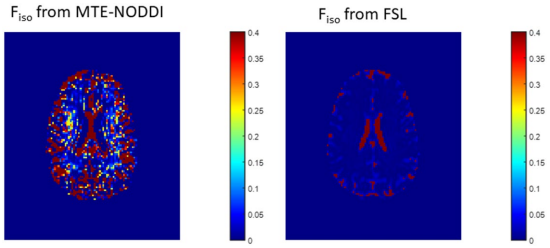

FIGURE 10
Representative maps of the fraction of the isotropic diffusion component (F_{iso}), that is, the cerebrospinal fluid fraction, derived using MTE-NODDI (left) or using the FAST algorithm as implemented in the FSL software (right). Results are shown for a representative slice.

incorporate signal fractions, it remains insensitive to differences in the CSF variation.

There are various techniques available to estimate NDI or ODI from single-shell or multishell DTI data (56, 69, 93–95). One of these techniques is the NODDI-DTI which assumes null CSF fractions in the WM (95). This contrasts with C-NODDI that uses the isotropic water fraction as a known pre-determined parameter. Interestingly, unlike C-NODDI, NODDI-DTI provides NDI values that are similar to those derived using NODDI. However, NODDI-DTI provides a unique approach to approximate NDI values from single-shell DTI, which has been used before by our group to reduce the scan time needed for whole-brain aggregate g-ratio mapping (30). However, it is important to acknowledge that all these methods are based on model simplifications, biophysical assumptions, fixed parameters, or complex fitting approaches, which may lack validation, stability, or clinical practicality (96, 97). However, there is a great deal of research currently toward further validation of these assumptions especially in preclinical research for more accurate determination of NDI or ODI. While challenging, more work must be conducted to make these techniques truly translatable to clinical investigations (98, 99). We believe that our approach introduced here for physiologically plausible NDI value and the validation against NfL opens the way for further developments to improve the NODDI modeling.

Our work has limitations. Although our cohort spans a wide age range, it does not include participants under the age of 20 due to the inclusion and exclusion criteria of the BLSA and GESTALT studies. Including younger participants may influence the shape of the NDI or ODI age-related trends and the assessment of their respective maxima with respect to age (100). With our current dataset being cross-sectional, our results could be further validated through longitudinal studies; such work is underway. In addition, the NODDI and C-NODDI implementations are based on several assumptions and fixed values for certain diffusivity parameters to improve the stability of the signal model. Further analyses are needed to investigate the effects of these fixed parameters on the NODDI and C-NODDI outcomes. Moreover, our acquisition protocol included only one image at b-value of 0 s/mm^2. However, it has been shown that several b_0 images are critical for an accurate determination of diffusion parameters (101). We also note that NODDI and C-NODDI assume similar transverse relaxation times between the intracellular and extracellular water compartments. This assumption is based on extensive relaxometry-based as well as diffusion-relaxometry-based work (58–61, 102). Although our results showing lower dependence of TE for C-NODDI derived NDI values in different brain regions support our assumption of relatively similar T_2s between the intra- and extra-cellular water compartments, other regions exhibit dependence to TE in agreement with previous work suggesting that these compartments exhibit different T_2s (56, 103). While our investigation has not yielded a definitive conclusion on this assumption, this observation highlights the complexity of brain microstructure and the potential limitations of a "one assumption fits all" approach given the fact that all these methods are simplifications based on biophysical assumptions that are often not validated or fitting approaches that are unstable which could lead to spurious results. We remain dedicated to further exploring this intriguing discrepancy within the existing literature. Finally, our method was applied to cognitively unimpaired individuals with further investigations required in the context of neurodegeneration and cognitive impairment. This is a proof-of-concept study, and further validation is warranted by acquiring data from different sites and scanners, as well as through post-mortem studies.

Data availability statement

The raw data supporting the conclusions of this article will be made available by the authors, without undue reservation.

Ethics statement

The studies involving human participants were reviewed and approved by the NIA ethics committee IRB. The patients/participants provided their written informed consent to participate in this study.

Author contributions

MB: theoretical and experimental design, data acquisition, results interpretation, and manuscript writing and editing. MA and ZG: data acquisition and analysis, results interpretation, and manuscript writing and editing. MK, CT, LC, MF, and JL: data analysis, results interpretation, and editing. CB: data acquisition and manuscript editing. All authors contributed to the article and approved the submitted version.

Conflict of interest

The authors declare that the research was conducted in the absence of any commercial or financial relationships that could be construed as a potential conflict of interest.

Publisher's note

All claims expressed in this article are solely those of the authors and do not necessarily represent those of their affiliated organizations, or those of the publisher, the editors and the reviewers. Any product that may be evaluated in this article, or claim that may be made by its manufacturer, is not guaranteed or endorsed by the publisher.

References

1. Peters A. The effects of normal aging on myelin and nerve fibers: a review. *J Neurocytol*. (2002) 31:581–93. doi: 10.1023/A:1025731309829

2. Tang Y, Nyengaard JR, Pakkenberg B, Gundersen HJ. Age-induced white matter changes in the human brain: a stereological investigation. *Neurobiol Aging*. (1997) 18:609–15. doi: 10.1016/S0197-4580(97)00155-3

3. Piguet O, Double KL, Kril JJ, Harasty J, Macdonald V, McRitchie DA, et al. White matter loss in healthy ageing: a postmortem analysis. *Neurobiol Aging*. (2009) 30:1288–95. doi: 10.1016/j.neurobiolaging.2007.10.015

4. Ghosh N, DeLuca G, Esiri M. Evidence of axonal damage in human acute demyelinating diseases. *J Neurol Sci*. (2004) 222:29–34. doi: 10.1016/j.jns.2004.03.032

5. Medana I, Esiri M. Axonal damage: a key predictor of outcome in human CNS diseases. *Brain*. (2003) 126:515–30. doi: 10.1093/brain/awg061

6. Beck D, de Lange A-MG, Maximov II, Richard G, Andreassen OA, Nordvik JE, et al. White matter microstructure across the adult lifespan: a mixed longitudinal and cross-sectional study using advanced diffusion models and brain-age prediction. *NeuroImage*. (2021) 224:117441. doi: 10.1016/j.neuroimage.2020.117441

7. Qian W, Khattar N, Cortina LE, Spencer RG, Bouhrara M. Nonlinear associations of neurite density and myelin content with age revealed using multicomponent diffusion and relaxometry magnetic resonance imaging. *NeuroImage*. (2020) 223:117369. doi: 10.1016/j.neuroimage.2020.117369

8. Salvadores N, Sanhueza M, Manque P, Court FA. Axonal degeneration during aging and its functional role in neurodegenerative disorders. *Front Neurosci*. (2017) 11. doi: 10.3389/fnins.2017.00451

9. Su KG, Banker G, Bourdette D, Forte M. Axonal degeneration in multiple sclerosis: the mitochondrial hypothesis. *Curr Neurol Neurosci Rep*. (2009) 9:411–7. doi: 10.1007/s11910-009-0060-3

10. Kanaan NM, Pigino GF, Brady ST, Lazarov O, Binder LI, Morfini GA. Axonal degeneration in Alzheimer's disease: when signaling abnormalities meet the axonal transport system. *Exp Neurol*. (2013) 246:44–53. doi: 10.1016/j.expneurol.2012.06.003

11. Lingor P, Koch JC, Tönges L, Bähr M. Axonal degeneration as a therapeutic target in the CNS. *Cell Tissue Res*. (2012) 349:289–311. doi: 10.1007/s00441-012-1362-3

12. Gong Z, Bilgel M, Kiely M, Triebswetter C, Ferrucci L, Resnick SM, et al. Lower myelin content is associated with more rapid cognitive decline among cognitively unimpaired individuals. *Alzheimers Dement*. (2023). doi: 10.1002/alz.12968

13. Inano S, Takao H, Hayashi N, Abe O, Ohtomo K. Effects of age and gender on white matter integrity. *AJNR Am J Neuroradiol*. (2011) 32:2103–9. doi: 10.3174/ajnr.A2785

14. Bartzokis G, Cummings JL, Sultzer D, Henderson VW, Nuechterlein KH, Mintz J. White matter structural integrity in healthy aging adults and patients with Alzheimer disease: a magnetic resonance imaging study. *Arch Neurol*. (2003) 60:393–8. doi: 10.1001/archneur.60.3.393

15. Yeatman JD, Wandell BA, Mezer AA. Lifespan maturation and degeneration of human brain white matter. *Nat Commun*. (2014) 5:4932. doi: 10.1038/ncomms5932

16. Fjell AM, Engvig A, Tamnes CK, Grydeland H, Walhovd KB, Westlye LT, et al. Life-span changes of the human brain white matter: diffusion tensor imaging (DTI) and Volumetry. *Cereb Cortex*. (2009) 20:2055–68. doi: 10.1093/cercor/bhp280

17. Arshad M, Stanley JA, Raz N. Adult age differences in subcortical myelin content are consistent with protracted myelination and unrelated to diffusion tensor imaging indices. *NeuroImage*. (2016) 143:26–39. doi: 10.1016/j.neuroimage.2016.08.047

18. Sullivan EV, Pfefferbaum A. Diffusion tensor imaging and aging. *Neurosci Biobehav Rev*. (2006) 30:749–61. doi: 10.1016/j.neubiorev.2006.06.002

19. Saito N, Sakai O, Ozonoff A, Jara H. Relaxo-volumetric multispectral quantitative magnetic resonance imaging of the brain over the human lifespan: global and regional aging patterns. *Magn Reson Imaging*. (2009) 27:895–906. doi: 10.1016/j.mri.2009.05.006

20. Alisch JSR, Egan JM, Bouhrara M. Differences in the choroid plexus volume and microstructure are associated with body adiposity. *Front Endocrinol (Lausanne)*. (2022) 13:984929. doi: 10.3389/fendo.2022.984929

21. Alisch JSR, Kiely M, Triebswetter C, Alsameen MH, Gong Z, Khattar N, et al. Characterization of age-related differences in the human choroid plexus volume, microstructural integrity, and blood perfusion using multiparameter magnetic resonance imaging. *Front Aging Neurosci*. (2021) 13:734992. doi: 10.3389/fnagi.2021.734992

22. Bouhrara M, Avram AV, Kiely M, Trivedi A, Benjamini D. Adult lifespan maturation and degeneration patterns in gray and white matter: a mean apparent propagator (MAP) MRI study. *Neurobiol Aging*. (2022) 124:104–16. doi: 10.1016/j.neurobiolaging.2022.12.016

23. Bouhrara M, Cortina LE, Khattar N, Rejimon AC, Ajamu S, Cezayirli DS, et al. Maturation and degeneration of the human brainstem across the adult lifespan. *Aging (Albany NY)*. (2021) 13:14862–91. doi: 10.18632/aging.203183

24. Bouhrara M, Kim RW, Khattar N, Qian W, Bergeron CM, Melvin D, et al. Age-related estimates of aggregate g-ratio of white matter structures assessed using quantitative magnetic resonance neuroimaging. *Hum Brain Mapp*. (2021) 42:2362–73. doi: 10.1002/hbm.25372

25. Bouhrara M, Triebswetter C, Kiely M, Bilgel M, Dolui S, Erus G, et al. Association of cerebral blood flow with longitudinal changes in cerebral microstructural integrity in the coronary artery risk development in young adults (CARDIA) study. *JAMA Netw Open*. (2022) 5:e2231189. doi: 10.1001/jamanetworkopen.2022.31189

26. Faulkner ME, Laporte JP, Gong Z, Akhonda M, Triebswetter C, Kiely M, et al. Lower myelin content is associated with lower gait speed in cognitively unimpaired adults. *J. Gerontol*. (2023). doi: 10.1093/gerona/glad080

27. Kiely M, Triebswetter C, Cortina LE, Gong Z, Alsameen MH, Spencer RG, et al. Insights into human cerebral white matter maturation and degeneration across the adult lifespan. *NeuroImage*. (2022) 247:118727. doi: 10.1016/j.neuroimage.2021.118727

28. Kiely M, Triebswetter C, Gong Z, Laporte JP, Faulkner ME, Akhonda M, et al. Evidence of An association between cerebral blood flow and microstructural integrity in normative aging using a holistic MRI approach. *J. Magnet. Resonan. Imaging*. (2022) 58:284–93. doi: 10.1002/jmri.28508

29. Laporte JP, Faulkner ME, Gong Z, Akhonda M, Ferrucci L, Egan JM, et al. Hypertensive adults exhibit lower myelin content: a multicomponent Relaxometry and diffusion magnetic resonance imaging study. *Hypertension*. (2023) doi: 10.1161/HYPERTENSIONAHA.123.21012

30. Cortina LE, Kim RW, Kiely M, Triebswetter C, Gong Z, Alsameen MH, et al. Cerebral aggregate g-ratio mapping using magnetic resonance relaxometry and diffusion tensor imaging to investigate sex and age-related differences in white matter microstructure. *Magn Reson Imaging*. (2022) 85:87–92. doi: 10.1016/j.mri.2021.10.019

31. Walker KA, Duggan MR, Gong Z, Dark HE, Laporte JP, Faulkner ME, et al. MRI and fluid biomarkers reveal determinants of myelin and axonal loss with aging. *Ann. Clin. Transl. Neurol*. (2023) 10:397–407. doi: 10.1002/acn3.51730

32. Zhang H, Schneider T, Wheeler-Kingshott CA, Alexander DC. NODDI: practical in vivo neurite orientation dispersion and density imaging of the human brain. *NeuroImage*. (2012) 61:1000–16. doi: 10.1016/j.neuroimage.2012.03.072

33. Timmers I, Roebroeck A, Bastiani M, Jansma B, Rubio-Gozalbo E, Zhang H. Assessing microstructural substrates of white matter abnormalities: a comparative study using DTI and NODDI. *PLoS One*. (2016) 11:e0167884. doi: 10.1371/journal.pone.0167884

34. Timmers I, Zhang H, Bastiani M, Jansma BM, Roebroeck A, Rubio-Gozalbo ME. White matter microstructure pathology in classic galactosemia revealed by neurite orientation dispersion and density imaging. *J Inherit Metab Dis*. (2015) 38:295–304. doi: 10.1007/s10545-014-9780-x

35. Mitchell T, Archer DB, Chu WT, Coombes SA, Lai S, Wilkes BJ, et al. Neurite orientation dispersion and density imaging (NODDI) and free-water imaging in parkinsonism. *Hum Brain Mapp*. (2019) 40:5094–107. doi: 10.1002/hbm.24760

36. Churchill NW, Caverzasi E, Graham SJ, Hutchison MG, Schweizer TA. White matter microstructure in athletes with a history of concussion: comparing diffusion tensor imaging (DTI) and neurite orientation dispersion and density imaging (NODDI). *Hum Brain Mapp*. (2017) 38:4201–11. doi: 10.1002/hbm.23658

37. Churchill NW, Caverzasi E, Graham SJ, Hutchison MG, Schweizer TA. White matter during concussion recovery: comparing diffusion tensor imaging (DTI) and neurite orientation dispersion and density imaging (NODDI). *Hum Brain Mapp*. (2019) 40:1908–18. doi: 10.1002/hbm.24500

38. By S, Xu J, Box BA, Bagnato FR, Smith SA. Application and evaluation of NODDI in the cervical spinal cord of multiple sclerosis patients. *Neuroimage Clin*. (2017) 15:333–42. doi: 10.1016/j.nicl.2017.05.010

39. Adluru G, Gur Y, Anderson JS, Richards LG, Adluru N, DiBella EV. Assessment of white matter microstructure in stroke patients using NODDI. *Conf Proc IEEE Eng Med Biol Soc*. (2014) 2014:742–5. doi: 10.1109/EMBC.2014.6943697

40. Winston GP, Micallef C, Symms MR, Alexander DC, Duncan JS, Zhang H. Advanced diffusion imaging sequences could aid assessing patients with focal cortical dysplasia and epilepsy. *Epilepsy Res*. (2014) 108:336–9. doi: 10.1016/j.eplepsyres.2013.11.004

41. Wen Q, Kelley DA, Banerjee S, Lupo JM, Chang SM, Xu D, et al. Clinically feasible NODDI characterization of glioma using multiband EPI at 7 T. *Neuroimage Clin*. (2015) 9:291–9. doi: 10.1016/j.nicl.2015.08.017

42. Kunz N, Zhang H, Vasung L, O'Brien KR, Assaf Y, Lazeyras F, et al. Assessing white matter microstructure of the newborn with multi-shell diffusion MRI and biophysical compartment models. *NeuroImage*. (2014) 96:288–99. doi: 10.1016/j.neuroimage.2014.03.057

43. Billiet T, Vandenbulcke M, Madler B, Peeters R, Dhollander T, Zhang H, et al. Age-related microstructural differences quantified using myelin water imaging and advanced diffusion MRI. *Neurobiol Aging*. (2015) 36:2107–21. doi: 10.1016/j.neurobiolaging.2015.02.029

44. Chang YS, Owen JP, Pojman NJ, Thieu T, Bukshpun P, Wakahiro ML, et al. White matter changes of neurite density and Fiber orientation dispersion during human brain maturation. *PLoS One*. (2015) 10:e0123656. doi: 10.1371/journal.pone.0123656

45. Nazeri A, Chakravarty MM, Rotenberg DJ, Rajji TK, Rathi Y, Michailovich OV, et al. Functional consequences of neurite orientation dispersion and density in humans across the adult lifespan. *J Neurosci*. (2015) 35:1753–62. doi: 10.1523/JNEUROSCI.3979-14.2015

46. Merluzzi AP, Dean DC 3rd, Adluru N, Suryawanshi GS, Okonkwo OC, Oh JM, et al. Age-dependent differences in brain tissue microstructure assessed with neurite orientation dispersion and density imaging. *Neurobiol Aging*. (2016) 43:79–88. doi: 10.1016/j.neurobiolaging.2016.03.026

47. Kodiweera C, Alexander AL, Harezlak J, McAllister TW, Wu YC. Age effects and sex differences in human brain white matter of young to middle-aged adults: a DTI, NODDI, and q-space study. *NeuroImage*. (2016) 128:180–92. doi: 10.1016/j.neuroimage.2015.12.033

48. Grussu F, Schneider T, Zhang H, Alexander DC, Wheeler-Kingshott CA. Neurite orientation dispersion and density imaging of the healthy cervical spinal cord in vivo. *NeuroImage*. (2015) 111:590–601. doi: 10.1016/j.neuroimage.2015.01.045

49. Jelescu IO, Veraart J, Adisetiyo V, Milla SS, Novikov DS, Fieremans E. One diffusion acquisition and different white matter models: how does microstructure change in human early development based on WMTI and NODDI? *NeuroImage*. (2015) 107:242–56. doi: 10.1016/j.neuroimage.2014.12.009

50. Grussu F, Schneider T, Tur C, Yates RL, Tachrount M, Ianuş A, et al. Neurite dispersion: a new marker of multiple sclerosis spinal cord pathology? *Ann Clin Transl Neurol*. (2017) 4:663–79. doi: 10.1002/acn3.445

51. Motovylyak A, Vogt NM, Adluru N, Ma Y, Wang R, Oh JM, et al. Age-related differences in white matter microstructure measured by advanced diffusion MRI in healthy older adults at risk for Alzheimer's disease. *Aging Brain*. (2022) 2:100030. doi: 10.1016/j.nbas.2022.100030

52. Raghavan S, Reid RI, Przybelski SA, Lesnick TG, Graff-Radford J, Schwarz CG, et al. Diffusion models reveal white matter microstructural changes with ageing, pathology and cognition. *Brain Commun*. (2021) 3. doi: 10.1093/braincomms/fcab106

53. Raghavan S, Przybelski SA, Reid RI, Lesnick TG, Ramanan VK, Botha H, et al. White matter damage due to vascular, tau, and TDP-43 pathologies and its relevance to cognition. *Acta Neuropathol Commun*. (2022) 10:16. doi: 10.1186/s40478-022-01319-6

54. Slattery CF, Zhang J, Paterson RW, Foulkes AJM, Carton A, Macpherson K, et al. ApoE influences regional white-matter axonal density loss in Alzheimer's disease. *Neurobiol Aging*. (2017) 57:8–17. doi: 10.1016/j.neurobiolaging.2017.04.021

55. Lawrence KE, Nabulsi L, Santhalingam V, Abaryan Z, Villalon-Reina JE, Nir TM, et al. Age and sex effects on advanced white matter microstructure measures in 15,628 older adults: a UK biobank study. *Brain Imaging Behav*. (2021) 15:2813–23. doi: 10.1007/s11682-021-00548-y

56. Gong T, Tong Q, He H, Sun Y, Zhong J, Zhang H. MTE-NODDI: multi-TE NODDI for disentangling non-T2-weighted signal fractions from compartment-specific T2 relaxation times. *NeuroImage*. (2020) 217:116906. doi: 10.1016/j.neuroimage.2020.116906

57. Bouyagoub S, Dowell N, Hurley S, Wood TC, Cercignani M. *Overestimation of CSF fraction in NODDI: Possible correction techniques and the effect on neurite density and orientation dispersion measures*. Singapore: ISMRM (2016).

58. MacKay A, Whittall K, Adler J, Li D, Paty D, Graeb D. In vivo visualization of myelin water in brain by magnetic resonance. *Magn Reson Med*. (1994) 31:673–7. doi: 10.1002/mrm.1910310614

59. MacKay AL, Laule C. Magnetic resonance of myelin water: An in vivo marker for myelin. *Brain Plasticity*. (2016) 2:71–91. doi: 10.3233/BPL-160033

60. Alonso-Ortiz E, Levesque IR, Pike GB. MRI-based myelin water imaging: a technical review. *Magn Reson Med*. (2015) 73:70–81. doi: 10.1002/mrm.25198

61. Does MD. Inferring brain tissue composition and microstructure via MR relaxometry. *NeuroImage*. (2018) 182:136–48. doi: 10.1016/j.neuroimage.2017.12.087

62. Alirezaei Z, Pourhanifeh MH, Borran S, Nejati M, Mirzaei H, Hamblin MR. Neurofilament light chain as a biomarker, and correlation with magnetic resonance imaging in diagnosis of CNS-related disorders. *Mol Neurobiol*. (2020) 57:469–91. doi: 10.1007/s12035-019-01698-3

63. Kölliker Frers RA, Otero-Losada M, Kobiec T, Udovin LD, Aon Bertolino ML, Herrera MI, et al. Multidimensional overview of neurofilament light chain contribution to comprehensively understanding multiple sclerosis. *Front Immunol*. (2022) 13:912005. doi: 10.3389/fimmu.2022.912005

64. Yik JT, Becquart P, Gill J, Petkau J, Traboulsee A, Carruthers R, et al. Serum neurofilament light chain correlates with myelin and axonal magnetic resonance imaging markers in multiple sclerosis. *Mult Scler Relat Disord*. (2022) 57:103366. doi: 10.1016/j.msard.2021.103366

65. Wang Z, Wang R, Li Y, Li M, Zhang Y, Jiang L, et al. Plasma Neurofilament light chain as a predictive biomarker for post-stroke cognitive impairment: a prospective cohort study. Frontiers in aging. *Neuroscience*. (2021) 13:13. doi: 10.3389/fnagi.2021.631738

66. Khalil M, Pirpamer L, Hofer E, Voortman MM, Barro C, Leppert D, et al. Serum neurofilament light levels in normal aging and their association with morphologic brain changes. *Nat Commun*. (2020) 11:812. doi: 10.1038/s41467-020-14612-6

67. O'Brien RJ, Resnick SM, Zonderman AB, Ferrucci L, Crain BJ, Pletnikova O, et al. Neuropathologic studies of the Baltimore longitudinal study of aging (BLSA). *J Alzheimers Dis*. (2009) 18:665–75. doi: 10.3233/JAD-2009-1179

68. Bouhrara M, Reiter DA, Maring MC, Bonny JM, Spencer RG. Use of the NESMA filter to improve myelin water fraction mapping with brain MRI. *J. Neuroimaging*. (2018) 28:640–9. doi: 10.1111/jon.12537

69. Veraart J, Novikov DS, Fieremans E. TE dependent diffusion imaging (TEdDI) distinguishes between compartmental T(2) relaxation times. *NeuroImage*. (2018) 182:360–9. doi: 10.1016/j.neuroimage.2017.09.030

70. Waterfall JJ, Casey FP, Gutenkunst RN, Brown KS, Myers CR, Brouwer PW, et al. Sloppy-model universality class and the Vandermonde matrix. *Phys Rev Lett*. (2006) 97. doi: 10.1103/PhysRevLett.97.150601

71. Transtrum MK, Machta BB, Sethna JP. Why are nonlinear fits to data so challenging? *Phys Rev Lett*. (2010) 104:060201. doi: 10.1103/PhysRevLett.104.060201

72. Bouhrara M, Reiter DA, Celik H, Fishbein KW, Kijowski R, Spencer RG. Analysis of mcDESPOT- and CPMG-derived parameter estimates for two-component nonexchanging systems. *Magn Reson Med*. (2016) 75:2406–20. doi: 10.1002/mrm.25801

73. Gutenkunst RN, Waterfall JJ, Casey FP, Brown KS, Myers CR, Sethna JP. Universally sloppy parameter sensitivities in systems biology models. *PLoS Comput Biol*. (2007) 3:1871–8. doi: 10.1371/journal.pcbi.0030189

74. Zhang Y, Brady M, Smith S. Segmentation of brain MR images through a hidden Markov random field model and the expectation-maximization algorithm. *IEEE Trans Med Imaging*. (2001) 20:45–57. doi: 10.1109/42.906424

75. Jenkinson M, Beckmann CF, Behrens TE, Woolrich MW, Smith SM. FSL. *FSL Neuroimage*. (2012) 62:782–90. doi: 10.1016/j.neuroimage.2011.09.015

76. Kazemi K, Noorizadeh N. Quantitative comparison of SPM, FSL, and Brainsuite for brain MR image segmentation. *J Biomed Phys Eng*. (2014) 4:13–26.

77. Hore P, Hall LO, Goldgof DB, Gu Y, Maudsley AA, Darkazanli A. A scalable framework for segmenting magnetic resonance images. *J Signal Process Syst*. (2009) 54:183–203. doi: 10.1007/s11265-008-0243-1

78. Bouix S, Martin-Fernandez M, Ungar L, Nakamura M, Koo MS, McCarley RW, et al. On evaluating brain tissue classifiers without a ground truth. *NeuroImage*. (2007) 36:1207–24. doi: 10.1016/j.neuroimage.2007.04.031

79. Mohammadi S, Möller HE, Kugel H, Müller DK, Deppe M. Correcting eddy current and motion effects by affine whole-brain registrations: evaluation of three-dimensional distortions and comparison with slicewise correction. *Magn Reson Med*. (2010) 64:1047–56. doi: 10.1002/mrm.22501

80. Benjamini Y. Discovering the false discovery rate. *J R Stat Soc Series B*. (2010) 72:405–16. doi: 10.1111/j.1467-9868.2010.00746.x

81. Benjamini Y, Hochberg Y. Controlling the false discovery rate: a practical and powerful approach to multiple testing. *J R Stat Soc Series B*. (1995) 57:289–300. doi: 10.1111/j.2517-6161.1995.tb02031.x

82. Golub M, Neto Henriques R, Gouveia NR. Free-water DTI estimates from single b-value data might seem plausible but must be interpreted with care. *Magn Reson Med*. (2021) 85:2537–51. doi: 10.1002/mrm.28599

83. Tristán-Vega A, París G, de Luis-García R, Aja-Fernández S. Accurate free-water estimation in white matter from fast diffusion MRI acquisitions using the spherical means technique. *Magn Reson Med*. (2022) 87:1028–35. doi: 10.1002/mrm.28997

84. Faiyaz A, Doyley M, Schifitto G, Zhong J, Uddin MN. Single-shell NODDI using dictionary-learner-estimated isotropic volume fraction. *NMR Biomed*. (2022) 35:e4628. doi: 10.1002/nbm.4628

85. Parker D, Ould Ismail AA, Wolf R, Brem S, Alexander S, Hodges W, et al. Freewater estimator using interpolated initialization (FERNET): characterizing peritumoral edema using clinically feasible diffusion MRI data. *PLoS One*. (2020) 15:e0233645. doi: 10.1371/journal.pone.0233645

86. Cox SR, Ritchie SJ, Tucker-Drob EM, Liewald DC, Hagenaars SP, Davies G, et al. Ageing and brain white matter structure in 3,513 UK biobank participants. *Nat Commun*. (2016) 7:13629. doi: 10.1038/ncomms13629

87. Westlye LT, Walhovd KB, Dale AM, Bjørnerud A, Due-Tønnessen P, Engvig A, et al. Life-span changes of the human brain white matter: diffusion tensor imaging (DTI) and volumetry. *Cereb Cortex*. (2010) 20:2055–68. doi: 10.1093/cercor/bhp280

88. Bouhrara M, Rejimon AC, Cortina LE, Khattar N, Bergeron CM, Ferrucci L, et al. Adult brain aging investigated using BMC-mcDESPOT based myelin water fraction imaging. *Neurobiol Aging*. (2020) 85:131–9. doi: 10.1016/j.neurobiolaging.2019.10.003

89. Dvorak AV, Swift-LaPointe T, Vavasour IM, Lee LE, Abel S, Russell-Schulz B, et al. An atlas for human brain myelin content throughout the adult life span. *Sci Rep*. (2021) 11:269. doi: 10.1038/s41598-020-79540-3

90. Mensch S, Baraban M, Almeida R, Czopka T, Ausborn J, El Manira A, et al. Synaptic vesicle release regulates myelin sheath number of individual oligodendrocytes in vivo. *Nat Neurosci*. (2015) 18:628–30. doi: 10.1038/nn.3991

91. Wake H, Lee PR, Fields RD. Control of local protein synthesis and initial events in myelination by action potentials. *Science*. (2011) 333:1647–51. doi: 10.1126/science.1206998

92. Simons M, Nave K-A. Oligodendrocytes: Myelination and axonal support. *Cold Spring Harb Perspect Biol*. (2015) 8:a020479. doi: 10.1101/cshperspect.a020479

93. Lampinen B, Szczepankiewicz F, Mårtensson J, van Westen D, Sundgren PC, Nilsson M. Neurite density imaging versus imaging of microscopic anisotropy in

diffusion MRI: a model comparison using spherical tensor encoding. *NeuroImage*. (2017) 147:517–31. doi: 10.1016/j.neuroimage.2016.11.053

94. Kaden E, Kelm ND, Carson RP, Does MD, Alexander DC. Multi-compartment microscopic diffusion imaging. *NeuroImage*. (2016) 139:346–59. doi: 10.1016/j.neuroimage.2016.06.002

95. Edwards LJ, Pine KJ, Ellerbrock I, Weiskopf N, Mohammadi S. NODDI-DTI: estimating neurite orientation and dispersion parameters from a diffusion tensor in healthy white matter. *Front Neurosci*. (2017) 11:720. doi: 10.3389/fnins.2017.00720

96. Jelescu IO, Veraart J, Fieremans E, Novikov DS. Degeneracy in model parameter estimation for multi-compartmental diffusion in neuronal tissue. *NMR Biomed*. (2016) 29:33–47. doi: 10.1002/nbm.3450

97. Jelescu IO, Palombo M, Bagnato F, Schilling KG. Challenges for biophysical modeling of microstructure. *J Neurosci Methods*. (2020) 344:108861. doi: 10.1016/j.jneumeth.2020.108861

98. Lampinen B, Szczepankiewicz F, Mårtensson J, van Westen D, Hansson O, Westin CF, et al. Towards unconstrained compartment modeling in white matter using diffusion-relaxation MRI with tensor-valued diffusion encoding. *Magn Reson Med*. (2020) 84:1605–23. doi: 10.1002/mrm.28216

99. Lampinen B, Szczepankiewicz F, Novén M, van Westen D, Hansson O, Englund E, et al. Searching for the neurite density with diffusion MRI: challenges for biophysical modeling. *Hum Brain Mapp*. (2019) 40:2529–45. doi: 10.1002/hbm.24542

100. Fjell AM, Walhovd KB, Westlye LT, Ostby Y, Tamnes CK, Jernigan TL, et al. When does brain aging accelerate? Dangers of quadratic fits in cross-sectional studies. *NeuroImage*. (2010) 50:1376–83. doi: 10.1016/j.neuroimage.2010.01.061

101. Jones DK, Horsfield MA, Simmons A. Optimal strategies for measuring diffusion in anisotropic systems by magnetic resonance imaging. *Magn Reson Med*. (1999) 42:515–25. doi: 10.1002/(SICI)1522-2594(199909)42:3<515::AID-MRM14>3.0.CO;2-Q

102. Benjamini D, Basser PJ. Use of marginal distributions constrained optimization (MADCO) for accelerated 2D MRI relaxometry and diffusometry. *J Magnet Res*. (1997) 271:40–5. doi: 10.1016/j.jmr.2016.08.004

103. Veraart J, Novikov DS, Fieremans E. TE dependent diffusion imaging (TEdDI) distinguishes between compartmental T2 relaxation times. *NeuroImage*. (2018) 182:360–9. doi: 10.1016/j.neuroimage.2017.09.030